Science and Technology Indonesia
e-ISSN:2580-4391 *p*-ISSN:2580-4405
Vol. 10, No. 3, July 2025

Research Paper

Performance of ZnS and ZnSe Doped on Cu^{2+} for Photovoltaic Devices

Le Xuan Thuy[1], Ha Thanh Tung[1*], Le Tien Dat[2], Le Minh Nhan[3]

[1]*Faculty of Basic Sciences, Vinh Long University of Technology Education, Vinh Long City, 85000, Vietnam*
[2]*University of Cuu Long, Vinh Long City, 85000, Vietnam*
[3]*Department of Chemistry, Faculty of Basic Sciences, Can Tho University of Medicine and Pharmacy, Can Tho, 94000, Vietnam*
***Corresponding author**: tunght@vlute.edu.vn

Abstract
This study utilizes passive ZnS@Cu^{2+} and ZnSe@Cu^{2+} layers deposited on the CdS and CdSe quantum dots to reduce dark current and enhance photon absorption. The films were fabricated utilizing the successive ionic layer adsorption and reaction technique with an optimized and suitable Cu/Zn doping ratio. Ultraviolet–visible spectroscopy, X-ray diffraction, and field emission scanning electron microscopy analyses indicate a change in the absorption edge within the visible light region when ZnS and ZnSe are doped with Cu^{2+} ions. Power conversion efficiency measurements reveal that the ZnSe@Cu^{2+} photoelectrode increases the current density (JSC ~23 mA.cm^{-2}) compared to ZnS@Cu^{2+} The photoelectrode exhibits a short-circuit current density ($J_{SC} \approx 22\ \mathrm{mA \cdot cm^{-2}}$), leading to improved conversion efficiency. It also shows the lowest charge transfer resistance ($R_{ct2} = 33 - \Omega$), indicating efficient interfacial kinetics in the photoelectrode suggests more efficient electron transport and reduced recombination.

Keywords
ZnS Nano, ZnSe Nano, Passivated Layers, Recombination

Received: 8 February 2025, Accepted: 27 May 2025
https://doi.org/10.26554/sti.2025.10.3.952-957

1. INTRODUCTION

Solar cells (SCs) are photovoltaic devices that convert light into electricity, operating based on the semiconductor phenomenon of photon absorption, generating electron-hole pairs (excitons), and producing an electric current. To improve efficiency and reduce costs, SCs have evolved through three generations: First Generation: Monocrystalline/polycrystalline silicon SCs with a theoretical efficiency of 31% (Shockley, 1961), achieving 15-25% in practice (Zhou et al., 2011), but with high costs due to the requirement for high-purity silicon; Second Generation: Thin-film SCs (CdTe, $CuInSe_2$, etc.) that reduce costs but have limited efficiency due to energy loss as heat; Third Generation: In 1991, Yella developed dye-sensitized solar cells (DSSCs) with a maximum efficiency of 13% (Yella et al., 2011). Later, nanotechnology led to a breakthrough with quantum dot-sensitized solar cells (QDSSCs), offering several advantages: Bandgap tunability based on quantum dot (QD) size, optimizing light absorption (Zhou et al., 2011; Kurniawan et al., 2025) high absorption coefficient due to quantum confinement effects (Yu et al., 2012); efficient exciton dissociation, enhancing charge carrier generation (Lee and Lo, 2009); multiple exciton generation (MEG) effect, enabling multiple excitons from a single high-energy photon (Lee and Lo, 2009). As a result, QDSSCs possess the ability to surpass the Shockley–Queisser efficiency upper bound (31%) and reach a theoretical efficiency of 44% (Hanna et al., 2012).

The layer of passivation plays a crucial role in forming an obstruction at the quantum dot and polysulfide interface, preventing the photogenerated electrons in QDs from recombining with the polysulfide (Chung et al., 2021; Jun and Tung, 2022). Common passivation materials include ZnS, ZnSe, SiO_2, Al_2O_3, and MgO, among which ZnS and ZnSe have been proven to be the most effective to enhance devices' power conversion efficiency (PCE) (Tyagi et al., 2021).

Copper is known as one of the metals with the lowest electrical resistance in nature. Therefore, doping Cu^{2+} ions into QDs has been proposed as a viable approach to enhancing QDSSCs performance (Muthalif et al., 2017). Studies on Cu^{2+} -doped QDs such as InP, ZnSe, CdS, and ZnS suggest that Cu^{2+} ions create an energy level closer to the valence band (VB) rather than the conduction band (CB), thereby slowing down excitons recombination and allowing QDs to absorb photons with energies lower than the bandgap. Additionally, unlike ultraviolet–visible spectroscopy of Mn-doped QDs, which are limited to the yellow-orange region, ultraviolet–visible spectroscopy of Cu-doped QDs can be tuned across the entire visible range depending on the QD size (Xie et al., 2014), demonstrating the potential for improving QDSSCs efficiency.

For the surface-passivated ZnS and ZnSe layers doped with metals used in the fabrication of QDSSCs, Lu and colleagues doped Mn into the surface-passivated ZnSe layer for CdS/CdSe QDSSCs and achieved a high power conversion efficiency of 6.46% (Lu et al., 2018). Similarly, Shen and collaborators used Mn-doped CdS/CdSe quantum dots, which improved the QDSSCs' efficiency to 5% (Shen et al., 2016). Gopi and colleagues employed Mn-doped ZnSe quantum dots and obtained a power conversion efficiency of 5.67% for the QDSSCs (Gopi et al., 2015). Phuc and co-workers doped Cu into CdS/CdSe quantum dots and achieved a power conversion efficiency of 4.23% (Phuc and Tung, 2018). These findings prove that transition metal doping of quantum dots (CdS, CdSe, ZnS, and ZnSe) is an efficient way to improve QDSSC performance.

In this study, we fabricated TiO_2/QDs/ZnS@Cu^{2+} and TiO_2/QDs/ZnSe@Cu^{2+} photoanodes for QDSSCs. The fabrication results are analyzed and discussed in detail in the discussion section of this paper.

2. EXPERIMENTAL SECTION

2.1 Materials

Na_2SO_3, NaOH, $Cd(CH_3COO)_2{\cdot}2H_2O$,$Zn(NO_3)_2$, $Na_2S{\cdot}9H_2O$, methanol, Se powder, $TiCl_4$, and $CuSO_4$ were purchased from Merck (Germany). Fluorine-doped tin oxide (FTO) glass substrates with a sheet resistance of 7 $\omega{\cdot}sq^{-1}$ and TiO_2 paste with a particle size of 20 nm were obtained from Dyesol (Australia).

2.2 Fabrication processes

2.2.1 Fabrication Process of FTO/TiO_2

The fluorine–doped tin oxide (FTO) conductive glass was cut into 1.2 cm × 2.0 cm pieces and cleaned by ultrasonic treatment in distilled water, 0.1M HCl, and ethanol. The TiO_2 layer was created using the screen-printing method: TiO_2 paste (Dyesol, 20 nm, Anatase) was spread through a mesh onto the conductive glass. Each layer was dried at 120°C for 10 minutes, repeated twice. The film was then gradually heated to 500°C maintained for 30 minutes, and naturally cooled to obtain a porous TiO_2 film.

2.2.2 Fabrication Process of FTO/TiO2/QDs (Van Thang et al., 2023)

The FTO/TiO_2 photoanode is alternately dipped in 0.1 M Cd^{2+} and 0.1 M S^{2-} solutions for 5 minutes each, followed by rinsing with ethanol and methanol. This completes one successive ionic layer adsorption and reaction (SILAR) cycle. A total of 3 cycles are performed, then the electrode is dried at 120°C for 15 minutes.

Mix Cd^{2+} and Cu^{2+} in 50 mL of ethanol and distilled water (1:1 ratio), let stand for 10 minutes, then combine. Dip the FTO/TiO_2/CdS electrode in a 0.1 M Cd^{2+} solution for 5 minutes, rinse with ethanol, then immerse it in a 0.3M Se^{-2} solution at 60°C for 5 minutes, and rinse with distilled water. Finally, dry the electrode at 120°C for 15 minutes.

The FTO/TiO2/QDs film is alternately dipped in 0.1M Zn^{2+} and Cu^{2+} and 0.1M S^{2-} (0.1M Se^{2-}) solutions for 5 minutes each, rinsing with distilled water after each step. The process is repeated twice, followed by drying the anode electrode at 120°C for 15 minutes.

2.2.3 Fabrication of Cu_2S

The anodizing process, heat-resistant tape is used to create a round hole and cover the conductive surface, allowing the Cu_2S layer to form only in the hole. Following a 30-minute deoxygenation with N_2 or Ar at 90°C, the taped FTO glass is cleaned with distilled water. Subsequently, it is immersed in a Cu^{2+} and S^{2-} solution. We finish by heating the Cu_2S film to 200°C, keeping it there for 30 minutes, and then letting it drop to room temperature (Van Thang et al., 2023).

2.2.4 Electrolyte

Create the polysulfide electrolyte system, 12 g of Na_2S, 0.64 g of sulfur (S), and 1.49 g of KCl were combined in 100 mL of a 7:3 volume ratio DI water/methanol (CH_3OH) solvent mixture. The final solution had a purple-yellow (Van Thang et al., 2023).

2.2.5 Fabrication of QDSSCs

The anode and cathode electrodes are assembled together with a transparent thermoplastic Surlyn sheet (25 μm thick) placed between them. This sheet has a circular hole with a diameter of 0.7 cm. The electrodes are held in place using clamps at two points. The assembly is then placed on a hot plate at 170°C and gently pressed so that the Surlyn melts, bonding the two electrodes together and expelling any air trapped in between. The polysulfide solution is injected into the cell through two pre-drilled holes in the cathode. The cell is then sealed with Surlyn, and a layer of silver is coated on both ends of the electrodes to enhance conductivity before measurement processes are carried out.

2.3 Characterization

Morphological examinations of the samples were carried out using Field Emission Scanning Electron Microscopy, also known as FE-SEM. The crystalline structures were characterized using an X-ray diffractometer (XRD, Philips, PANalytical X'Pert) equipped with CuKα radiation. In order to assess the optical absorption properties, JASCO V-670 UV-vis diffuse reflectance spectroscopy was used. Under simulated AM 1.5 sun light (100 $mW{\cdot}cm^{-2}$), which was provided by a Solarena solar simulator (Sweden), the photocurrent-voltage characteristics were measured using a Keithley 2400 source meter. Electrochemical impedance spectroscopy (EIS) was carried out using a ZAHNER CIMPS impedance analyzer.

3. RESULTS AND DISCUSSION

The FESEM surface image of the sample (Figure 1), taken at a resolution of 100 nm, reveals that the film has a highly porous structure, with particles averaging several tens of nanometers in

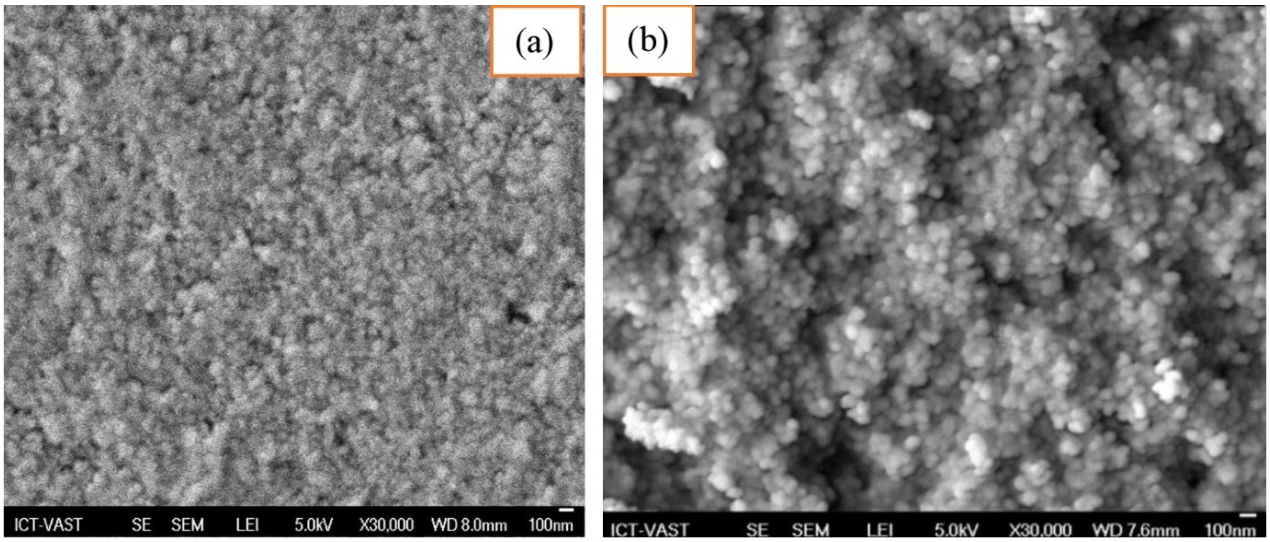

Figure 1. FESEM of (a) ZnS and (b) ZnSe Passivation Layers Doped- Cu^{2+}

Table 1. The Characteristic Parameters of Devices

Sample	V_{oc} (V)	J_{sc} (mA·cm^{-2})	FF	PCE (%)	R_{ct1} (Ω)	R_{ct2} (Ω)
TiO_2/QDs/ZnS@Cu^{2+}	0.515	22	0.41	4.5	12	116
TiO_2/QDs/ZnSe@Cu^{2+}	0.520	23	0.439	5.3	17	33

size. The TiO_2 film itself exhibits high porosity because of the relatively enormous TiO_2 particle size, resulting in numerous voids between them. Consequently, CdS, CdSe(Mn^{2+}), and ZnS nanoparticles can would readily absorb onto the TiO_2's surface nanoparticles. The surface of the film appears relatively uniform and free of cracks, as shown in the SEM image at ×500 magnification.

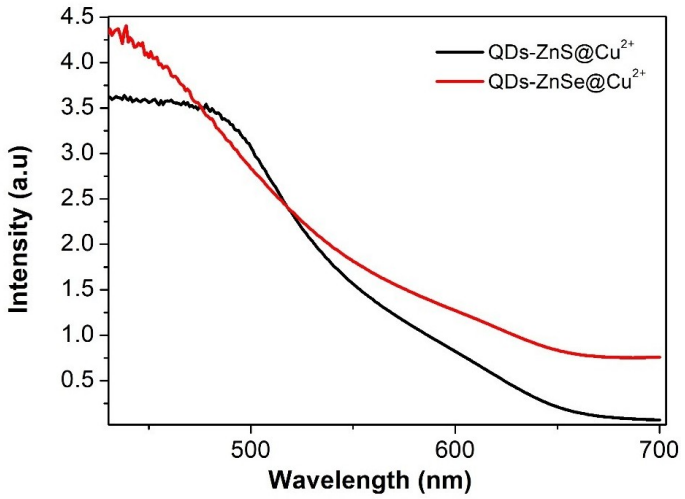

Figure 2. UV-Vis of of ZnS and ZnSe Passivation Layers Doped - Cu^{2+} at Optimal Conditions

Figure 2 shows the UV-Vis spectrum of the FTO/QDs photoanode doped with Cu^{3+}, which includes passivation layers of ZnS and ZnSe, in the 300-700 nm region. To demonstrate how the absorbance varies with the Cu^{2+} doping ratio, light is shone on the FTO substrate side. The production of Cu^{2+} energy levels within the bandgap of ZnS and ZnSe may explain why the absorption strength somewhat rises with Cu^{2+} presence below 550 nm. This result is consistent with Zahra's study on Sr doping in ZnSe for QDSSCs (Lu et al., 2018). The FTO/TiO_2/QDs/ZnSe@Cu^{2+} system exhibits enhanced absorption and a red shift in the 500–600 nm range. The FTO/-TiO_2/QDs/ZnSe@Cu^{2+} photoanode shows a higher absorption spectrum intensity than the FTO/TiO_2/QDs/ZnS@Cu^{2+} photoanode. Overall, the doped anode films absorb longer wavelengths, extend into the visible light region, and result in a darker material.

The structure of CdS, CdSe, ZnS@Cu^{2+}, and ZnSe@Cu^{2+} quantum dots on the TiO_2 surface is determined by X-ray diffraction analysis; all of these samples display crystallinity (Figure 3). According to JCPDS 00-004-0477, the five diffraction peaks of TiO_2 at 25.354°, 37.785°, 48.077°, 53.922°, and 62.728° represent the (101), (004), (200), (105), and (204) planes of the Anatase phase, respectively (Gopi et al., 2015). The cubic structure of CdS is identified through the (111) and (222) peaks at 26.5° and 54.5° (JCPDS 00-089-0440) (Shen et al., 2016; Gopi et al., 2015). Two peaks at 27.2° and 42° correspond to the (101) and (110) planes of hexagonal CdSe (JCPDS 00-008-0459) (Shen et al., 2016). Hexagonal ZnS and ZnSe exhibit two peaks at 25.7° and 48.8°, corresponding

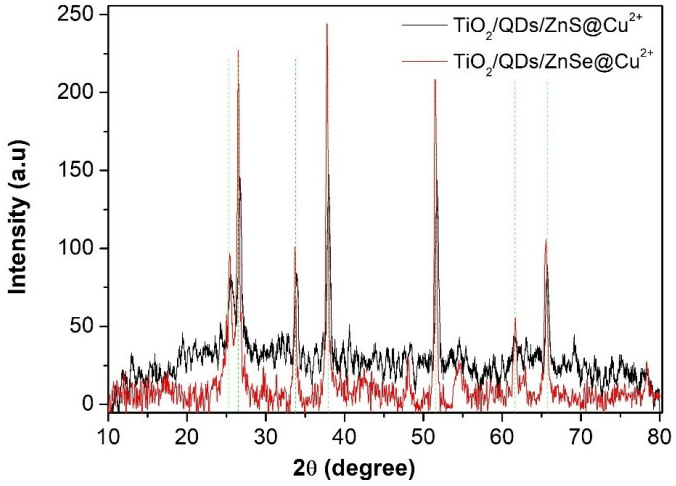

Figure 3. XRD Spectra of Zns and Znse Passivation Layers Doped - Cu^{2+} Photoanodes

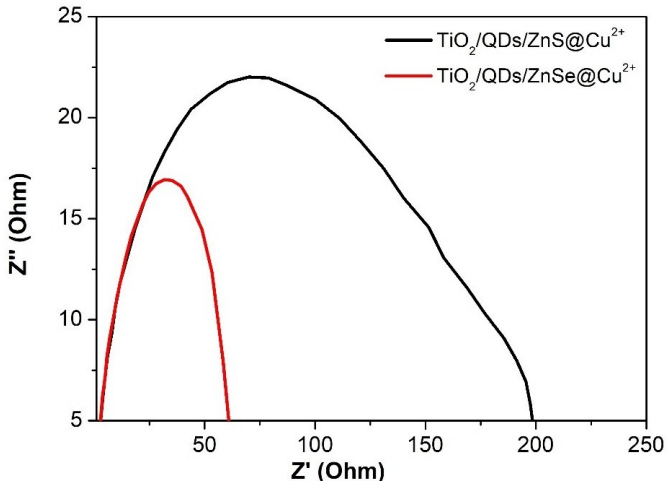

Figure 5. EIS of Qdsscs Based on Zns and Znse Passivation Layers Doped - Cu^{2+} Photoanodes

to the (100) and (103) planes (JCPDS 00-089-2940) (Lu et al., 2018). These results confirm the successful deposition of CdS, CdSe, and ZnSe onto TiO_2.

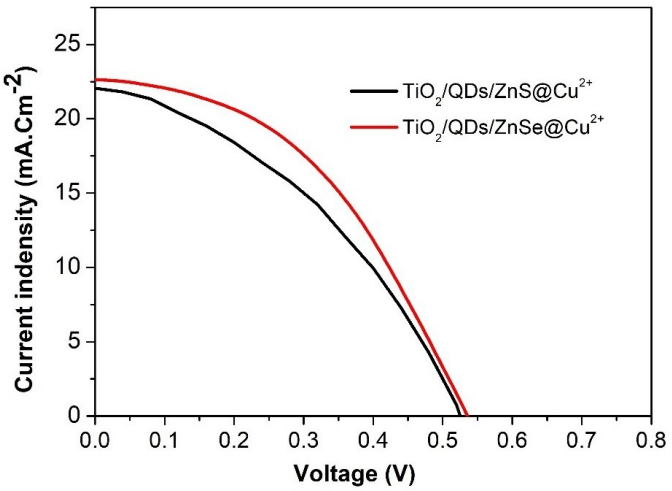

Figure 4. Photovoltaic Performance of Qdsscs Based on Zns and Znse Passivation Layers Doped - Cu^{2+} Photoanodes

We measured the photovoltaic performance curves (J–V) of QDSSCs with TiO_2/QDs/ZnS@Cu^{2+} and TiO_2/QDs/ZnSe@Cu^{2+} photoanodes under standard sunlight illumination of 100 mW.cm^{-2} (Figure 4 and Table 1). The results show that the open-circuit voltage (Voc) and fill factor (FF) remain nearly unchanged, but the conversion efficiency varies significantly with current density. For the TiO_2/QDs/ZnS@Cu^{2+} film, the current density reaches 22 mA.cm^{-2} with an efficiency of 4.5%, which is lower than that of TiO_2/QDs/ZnSe@Cu^{2+}. When Cu^{2+} is doped into TiO_2/QDs/ZnSe, the efficiency and current density increase significantly, reaching a maximum of 23 mA.cm^{-2} and 5.3%, respectively. This increase is attributed to Cu^{2+} substituting Zn^{2+} in the crystal lattice, leading to a reduction in film resistance and the formation of impurity energy levels in the bandgap of ZnS and ZnSe, enhancing photon absorption. This result is consistent with the study by Firoozi et al. (2018) in which doping Cu^{2+} and Mn^{2+} into ZnS significantly increased the current density.

The study investigates the electron transfer process in thin film layers, electron transfer at the photoanode interface (R_{ct2}), electron diffusion in the electrolyte, and electron transfer at the cathode (R_{ct1}) using electrochemical impedance spectroscopy under 100 MW.cm^{-2} illumination (Figure 5, Table 1). Analysis using EC-LAB software indicates that Cu^{2+} -doped ZnS-coated electrodes exhibit lower charge transfer resistances (R_{ct1}), (R_{ct2}) than Cu^{2+} -doped ZnSe, with minimum values of (R_{ct1}) = 17 ω and (R_{ct2}) = 33 ω. Simultaneously, the current density and efficiency significantly increase from 22 mA.cm^{-2} to 23 mA.cm^{-2}. This improvement is attributed to the ZnS@Cu^{+2} and ZnS@Cu^{+2} layers, which not only enhance photon absorption but also reflect light, enabling more efficient absorption by TiO_2/QDs (Phuc and Tung, 2018; Nguyen et al., 2021). Additionally, the conduction band of ZnS@Cu^{+2} and ZnS@Cu^{+2} is higher than that of TiO_2/QDs, reducing electron back diffusion and minimizing recombination (Van Thang et al., 2023; Beaulac et al., 2008). Cu^{+2} doping also shifts the absorption spectrum into the visible light region due to impurity energy levels within the bandgap of ZnS and ZnSe (Firoozi et al., 2018; Van Thang et al., 2023; Huang et al., 2016). These findings align with the research by Firoozi et al. (2018) and show a significantly higher efficiency compared to (Mo et al., 2017; Chandrakar et al., 2015; Rao et al., 2015; Zhu et al., 2021; Huang et al., 2017).

The QDSSCs based on ZnSe@Cu^{2+} achieved an efficiency (5.3%) comparable to that of (Zhang et al., 2015). Although Voc and FF are slightly lower, but Jsc is higher (23 mA per cm^2 compared to 16.2 mA per cm^2) (Zhang et al., 2015). The coat-

Table 2. Comparison of the Results Obtained in This Study with Those of Previous Research Groups

Refs	QDSSCs	V_{oc} (V)	J_{sc} (mA/cm^2)	FF	PCE (%)
(Lee et al., 2013) (ZnS passivation)	TiO_2/CdSe QDs/ZnS	0.54	14.0	0.55	4.2
(Zhang et al., 2015) (ZnSe shell)	TiO_2/CdSe/ZnSe	0.56	16.2	0.59	5.3
(He et al., 2016) (Cu^{2+} modification)	TiO_2/CdS/ZnS@Cu^{2+}	0.52	18.1	0.48	4.8
(Wang et al., 2019)	TiO_2/PbS/CdS/ZnS	0.48	25.0	0.42	5.1

ing of ZnSe and Cu^{2+} ions work together to improve electron transport and reduce recombination, as shown by the slight increase in the efficiency of the PCE (5.3%- >4.8%) compared to He et al. (2016) (Table 2). Compared to multi-layer systems such as PbS, CdS and ZnS, the results are comparable to those of QDSSCs systems with an efficiency of around 5 percent, especially when a simple structure (only one absorption layer) is used (He et al., 2016; Lee et al., 2013; Wang et al., 2019). Reduce the magnitude of the decrease in the denominator by decreasing the recombination. Replacing ZnSe with ZnS in the QDs structure along with Cu^{2+} ions greatly increases the photovoltaic efficiency. The cause of this result is better repression of recombination. Given the simplicity of the structure and materials used, the results achieved are comparable to or better than those of many previous studies etc.

4. CONCLUSIONS

The passivation layers ZnS@Cu^{2+} and ZnSe@Cu^{2+} were successfully fabricated using the SILAR method, effectively passivating the surface of CdS and CdSe quantum dots on the photoanode electrode while enhancing photon absorption in QDSSCs. The absorption spectrum reveals that the absorption peak of electrodes with ZnS@Cu^{2+} and ZnSe@Cu^{2+} shifts toward longer wavelengths in the visible region, consistent with the J-V spectrum results. The current density increases from 23 mA·cm^{-2}, and the efficiency improves from 5.3%, thanks to the support of ZnSe@Cu^{2+}. Electrochemical impedance spectroscopy confirms the lowest charge transfer resistance in ZnS@Cu^{2+}, which helps reduce recombination and improve electron transport. The structural, morphological, and thickness properties of the films were determined using XRD and FE-SEM.

5. ACKNOWLEDGMENT

The authors wish to express the colleagues for providing the resources and support needed to complete this study.

REFERENCES

Beaulac, R., P. I. Archer, X. Liu, S. Lee, G. M. Salley, M. Dobrowolska, and D. R. Gamelin (2008). Spin-Polarizable Excitonic Luminescence in Colloidal Mn^{2+}-Doped CdSe Quantum Dots. *Nano Letters*, **8**(4); 1197–1201

Chandrakar, R. K., R. N. Baghel, V. K. Chandra, and B. P. Chandra (2015). Synthesis, Characterization and Photoluminescence Studies of Mn Doped ZnS Nanoparticles. *Superlattices and Microstructures*, **86**; 256–269

Chung, N. T. K., P. T. Nguyen, H. T. Tung, and D. H. Phuc (2021). Quantum Dot Sensitized Solar Cell: Photoanodes, Counter Electrodes, and Electrolytes. *Molecules*, **26**(9); 2638

Firoozi, N., H. Dehghani, M. Afrooz, and S. S. Khalili (2018). Improvement Photovoltaic Performance of Quantum Dot-Sensitized Solar Cells Using Deposition of Metal-Doped ZnS Passivation Layer on the TiO_2 Photoanode. *Microelectronic Engineering*, **198**; 8–14

Gopi, C. V., M. Venkata-Haritha, S. K. Kim, and H. J. Kim (2015). A Strategy to Improve the Energy Conversion Efficiency and Stability of Quantum Dot-Sensitized Solar Cells Using Manganese-Doped Cadmium Sulfide Quantum Dots. *Dalton Transactions*, **44**(2); 630–638

Hanna, M. C., M. C. Beard, and A. J. Nozik (2012). Effect of Solar Concentration on the Thermodynamic Power Conversion Efficiency of Quantum-Dot Solar Cells Exhibiting Multiple Exciton Generation. *The Journal of Physical Chemistry Letters*, **3**(19); 2857–2862

He, Y., H. Zhong, W. Hu, and Y. Li (2016). Cu^{2+} Modified ZnS Layers for Enhanced Performance in Quantum Dot-Sensitized Solar Cells. *Materials Research Bulletin*, **79**; 67–72

Huang, F., J. Hou, H. Wang, H. Tang, Z. Liu, L. Zhang, and G. Cao (2017). Impacts of Surface or Interface Chemistry of ZnSe Passivation Layer on the Performance of CdS/CdSe Quantum Dot Sensitized Solar Cells. *Nano Energy*, **32**; 433–440

Huang, F., J. Hou, Q. Zhang, Y. Wang, R. C. Massé, S. Peng, and G. Cao (2016). Doubling the Power Conversion Efficiency in CdS/CdSe Quantum Dot Sensitized Solar Cells With a ZnSe Passivation Layer. *Nano Energy*, **26**; 114–122

Jun, H. K. and H. T. Tung (2022). A Short Overview on Recent Progress in Semiconductor Quantum Dot-Sensitized Solar Cells. *Journal of Nanomaterials*, **2022**(1); 1382580

Kurniawan, M. R. H., S. A. Cahyani, N. Kusumawati, P. Setiarso, and S. Muslim (2025). Optimization of Radiation and Electric Current Storage in a Dye-Sensitized Solar-Cell System Based FTO/TiO2 /Acy/PVDF/C/FTO Modules for Electrical Equipment Applications. *Science and Technology Indonesia*, **10**(2); 574–587

Lee, H., H. Choi, N. G. Park, and J. Y. Kim (2013). Improved Performance of Quantum Dot-Sensitized Solar Cells Using ZnS Passivation Layer. *Journal of Photochemistry and Photobiology A: Chemistry*, **253**; 150–156

Lee, Y. L. and Y. S. Lo (2009). Highly Efficient Quantum-

Dot-Sensitized Solar Cell Based on Co-Sensitization of CdS/CdSe. *Advanced Functional Materials*, **19**(4); 604–609

Lu, S., S. Peng, Z. Zhang, Y. Deng, T. Qin, J. Huang, and G. Cao (2018). Impacts of Mn Ion in ZnSe Passivation on Electronic Band Structure for High Efficiency CdS/CdSe Quantum Dot Solar Cells. *Dalton Transactions*, **47**(29); 9634–9642

Mo, Z. J., Z. H. Hao, J. Z. Deng, J. Shen, L. Li, J. F. Wu, and B. G. Shen (2017). Observation of Giant Magnetocaloric Effect Under Low Magnetic Field in $Eu_{1-x}Ba_xTiO_3$. *Journal of Alloys and Compounds*, **694**; 235–240

Muthalif, M. P. A., Y. S. Lee, C. D. Sunesh, H. J. Kim, and Y. Choe (2017). Enhanced Photovoltaic Performance of Quantum Dot-Sensitized Solar Cells With a Progressive Reduction of Recombination Using Cu-Doped CdS Quantum Dots. *Applied Surface Science*, **396**; 582–589

Nguyen, V., L. Yan, N. Zhao, N. Van Canh, N. T. N. Hang, and P. H. Le (2021). Tuning Photoluminescence of Boron Nitride Quantum Dots via Surface Functionalization by Femtosecond Laser Ablation. *Journal of Molecular Structure*, **1244**; 130922

Phuc, D. H. and H. T. Tung (2018). The Effect of Thickness on the Performance of CdSe:Cu^{2+}–Quantum Dot-Sensitized Solar Cells. *Applied Physics A*, **124**(11); 731

Rao, S. S., D. Punnoose, C. V. Tulasivarma, C. P. Kumar, C. V. Gopi, S. K. Kim, and H. J. Kim (2015). A Strategy to Enhance the Efficiency of Dye-Sensitized Solar Cells by the Highly Efficient TiO_2/ZnS Photoanode. *Dalton Transactions*, **44**(5); 2447–2455

Shen, T., J. Tian, L. Lv, C. Fei, Y. Wang, T. Pullerits, and G. Cao (2016). Investigation of the Role of Mn Dopant in CdS Quantum Dot Sensitized Solar Cell. *Electrochimica Acta*, **191**; 62–69

Shockley, W. (1961). Problems Related to PN Junctions in Silicon. *Solid-State Electronics*, **2**(1); 35–67

Tyagi, J., H. Gupta, and L. P. Purohit (2021). Ternary Alloyed $CdS_{1-x}Se_x$ Quantum Dots on TiO_2/ZnS Electrodes for Quantum Dots-Sensitized Solar Cells. *Journal of Alloys and Compounds*, **880**; 160480

Van Thang, B., H. T. Tung, D. H. Phuc, T. P. Nguyen, T. Van Man, and L. Q. Vinh (2023). High-Efficiency Quantum Dot Sensitized Solar Cells Based on Flexible rGO-Cu_2S Electrodes Compared With PbS, CuS, Cu_2S CEs. *Solar Energy Materials and Solar Cells*, **250**; 112042

Wang, Y., K. Chen, X. Liu, and J. Xu (2019). High Efficiency Quantum Dot-Sensitized Solar Cells Based on PbS/CdS/ZnS Structure. *Solar Energy Materials and Solar Cells*, **193**; 105–112

Xie, C., B. Nie, L. Zeng, F. X. Liang, M. Z. Wang, L. Luo, and S. H. Yu (2014). Core–Shell Heterojunction of Silicon Nanowire Arrays and Carbon Quantum Dots for Photovoltaic Devices and Self-Driven Photodetectors. *ACS Nano*, **8**(4); 4015–4022

Yella, A., H. W. Lee, H. N. Tsao, C. Yi, A. K. Chandiran, M. K. Nazeeruddin, and M. Grätzel (2011). Porphyrin-Sensitized Solar Cells With Cobalt (II/III)–Based Redox Electrolyte Exceed 12 Percent Efficiency. *Science*, **334**(6056); 629–634

Yu, X. Y., B. X. Lei, D. B. Kuang, and C. Y. Su (2012). High Performance and Reduced Charge Recombination of CdSe/CdS Quantum Dot-Sensitized Solar Cells. *Journal of Materials Chemistry*, **22**(24); 12058–12063

Zhang, Q., T. Zhang, and G. Cao (2015). Enhanced Efficiency of CdSe Quantum Dot Sensitized Solar Cells With ZnSe Shell. *Electrochimica Acta*, **176**; 844–851

Zhou, Y., M. Eck, C. Veit, B. Zimmermann, F. Rauscher, P. Niyamakom, and M. Krüger (2011). Efficiency Enhancement for Bulk-Heterojunction Hybrid Solar Cells Based on Acid Treated CdSe Quantum Dots and Low Bandgap Polymer PCPDTBT. *Solar Energy Materials and Solar Cells*, **95**(4); 1232–1237

Zhu, W., Y. Y. Hu, W. Wang, Y. Xie, W. Xue, F. He, and Y. Li (2021). Surface Engineering Boosting Al/Zn-Coincorporated Cu–In–Se Quantum Dot-Sensitized Solar Cell Efficiency. *ACS Applied Energy Materials*, **4**(6); 5767–5774

